Chapter 5
On the Effectiveness of Higher-Order One-Dimensional Models for Physically Nonlinear Problems

I. Kaleel, M. Petrolo, E. Carrera and A. M. Waas

Abstract The chapter presents numerical assessments of physically nonlinear problems through a class of refined one-dimensional theories based on the Carrera Unified Formulation (CUF). CUF is a hierarchical formulation to generate refined structural theories through a variable kinematic approach. Physical nonlinearities include von Mises plasticity and cohesive interface modeling for delamination of composites. This work aims to provide insights into the effect of kinematic enrichment on the overall nonlinear behavior of the structure. Guidelines stem from the evaluation of the accuracy and numerical efficiency of the proposed models against analytical and numerical approaches from the literature.

5.1 Introduction

The engineering practice tends to use simple analytical and finite element models for the stress analysis of structures to obtain computational efficiency and acceptable levels of accuracy. One-dimensional models (1D)—referred to as beams—fall within the scope of the analysis of slender structures such as columns, blades, and aircraft wings. Classical models such as Euler–Bernoulli (EBBT) [4, 12] and Timoshenko (TBT) [29] are common options for practical engineering analyses, but the effectiveness of such models depend on many assumptions such as geometrical dimensions, the prismatic nature of the structure, material homogeneity and isotropy. Since the accurate resolution of displacement and stress fields serves as a precursor for reliable nonlinear simulations, the validity of classical models in the nonlinear regime may be questionable and 2D, or 3D models are often mandatory with significant

I. Kaleel (✉) · M. Petrolo · E. Carrera
MUL2 Group, Department of Mechanical and Aerospace Engineering, Politecnico di Torino, Torino, Italy
e-mail: ibrahim.kaleel@polito.it

A. M. Waas
Department of Aerospace Engineering, University of Michigan Ann Arbor, Ann Arbor, MI, USA

M. Petrolo (ed.), *Advances in Predictive Models and Methodologies for Numerically Efficient Linear and Nonlinear Analysis of Composites*, PoliTO Springer Series,
https://doi.org/10.1007/978-3-030-11969-0_5

computational overheads. This chapter presents a novel approach in modeling the physical nonlinearities through higher-order 1D. Over the past few decades, significant efforts have led to the development of 1D models to solve diverse classes of physically nonlinear problems, and a brief overview follows.

Timoshenko and Gere extended the TBT to doubly-symmetric inelastic beams [30]. Abambres et al. employed the Generalized Beam Theory (GBT), originally developed by Schardt [25], for elastoplastic and post-buckling analyses of metallic thin-walled beam structures [1]. A class of 1D models stemmed from the Variational Asymptotic Beam Section Analysis (VABS), a variational asymptotic method which replaces a 3D structural model with a reduced-order model via asymptotic series [10]. The methodology also has nonlinear capabilities as shown by Pollayi et al. to model matrix cracking in helicopter rotors or wind turbine blades [23]. Jiang and Yu extended VABS to hyperelastic beams subjected to finite deformations and damage analyses of composites [16, 17]. Groh and Tessler developed a computationally efficient beam model to capture the delamination in laminated composite beams [14] via a nine degrees of freedom (DOF) and eight-DOF locking-free beam elements employing a mixed form of a refined zig-zag theory capturing the transverse stress field. Škec et al. [28] developed a 2D multilayered beam finite element for mixed-mode delamination analyses. Eijo et al. presented a method based on a refined zig-zag theory within a 1D finite element to model delamination in composite laminated beams [11].

The chapter deals with extensions of 1D CUF models for analyzing physically nonlinear problems and effectiveness concerning accuracy and computational efficiency. CUF is a hierarchical formulation that reduces 3D problems to 2D or 1D in a unified manner through a variable kinematic description [9]. The ability of 1D CUF models to recover accurate 3D stress fields efficiently can solve broad categories of physically nonlinear problems. Originally developed for plates and shells, 1D CUF models can deal with nonlinearities due to large deflections and post-buckling [22], elastoplastic and progressive damage analysis [8, 19, 20], and rotordynamics [13].

This chapter provides an overview of the nonlinear constitutive laws in Sect. 5.2, describes the structural modeling and FE framework in Sect. 5.3, highlights the most important aspects related to the solution schemes for nonlinear problems in Sect. 5.4, and shows results and comments in Sects. 5.5 and 5.6.

5.2 Nonlinear Constitutive Equations

The adopted Cartesian coordinate system has the beam axis along the y-axis and the cross-section along the $x - z$ plane. The displacement vector at any given point in the structural domain is

$$\mathbf{u}\,(x, y, z) = [u_x \quad u_y \quad u_z]^T \tag{5.1}$$

The vectorial notations for strain and stress states are

$$\boldsymbol{\varepsilon} = [\varepsilon_{xx} \quad \varepsilon_{yy} \quad \varepsilon_{zz} \quad \varepsilon_{yz} \quad \varepsilon_{xz} \quad \varepsilon_{xy}]^T; \quad \boldsymbol{\sigma} = [\sigma_{xx} \quad \sigma_{yy} \quad \sigma_{zz} \quad \sigma_{yz} \quad \sigma_{xz} \quad \sigma_{xy}]^T \tag{5.2}$$

Under the small strain assumption, geometrical and constitutive equations are

$$\boldsymbol{\varepsilon} = \mathbf{b}\,\mathbf{u}; \qquad \mathbf{b}^T = \begin{bmatrix} \partial_x & 0 & 0 & 0 & \partial_z & \partial_y \\ 0 & \partial_y & 0 & \partial_z & 0 & \partial_x \\ 0 & 0 & \partial_z & \partial_y & \partial_x & 0 \end{bmatrix}; \qquad \boldsymbol{\sigma} = \mathbf{C}\,\boldsymbol{\varepsilon} \tag{5.3}$$

where $\mathbf{b}$ is the differential operator and $\mathbf{C}$ reads a nonlinear generic constitutive material matrix with 36 constants to describe the stress-strain behavior.

5.2.1 Plasticity

The von Mises (J_2) theory hypothesizes that the material starts to yield when the J_2 invariant of the stress tensor attains a certain threshold, often referred to as the yield stress,

$$f = q(\boldsymbol{\sigma}) - \sigma_y(\bar{\varepsilon_p}) \tag{5.4}$$

where f is the von Mises yield locus, $q(\boldsymbol{\sigma})$ is the von Mises stress and σ_y is the yield stress which is a material input. A return mapping numerical scheme solves the local nonlinear problem, as detailed in Carrera et al. for CUF models [8]. In addition to metals, the nonlinear shear response exhibited by unidirectional laminates is due to inelastic deformation incurred by matrix constituents, often modeled through the von Mises based plasticity method.

5.2.2 Cohesive Modeling

Let us consider a domain Ω with a crack zone Γ_c as shown in Fig. 5.1. Essential boundary conditions act along the boundary Γ_u and prescribed tractions τ_i along Γ_n. The domain has two sub-domains, Ω_+ and Ω_-, along the crack boundary Γ_c, as depicted in Fig. 5.1. The equilibrium equations within the domain Ω are

$$\begin{aligned} \sigma_{ij,j} + \rho b_i = 0 \quad in \quad \Omega; \qquad \sigma_{ij} n_j = t_i \quad in \quad \Gamma_n \\ \sigma_{ij} n_j^+ = \tau_i^+ = -\tau_i^- = -\sigma_{ij} n_j^- n_j^- \quad in\ \Gamma_c \end{aligned} \tag{5.5}$$

where σ_{ij} is the stress field within the domain due to external loading $\mathbf{t}_i$, b_i are the body forces, ρ is the density of the material, and τ_i^+, τ_i^- are the closing tractions acting along the cohesive surface. Via the Principle of Virtual Displacements (PVD)

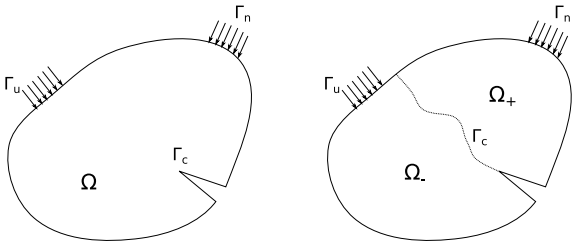

Fig. 5.1 Boundary value problem for cohesive formulation

and considering the additional contributions to work due to the cohesive crack, the weak formulation reads

$$\begin{aligned} &\delta L_{int} + \delta L_{coh} - \delta L_{ext} = 0, \quad \delta L_{int} = \int_{\Omega} \boldsymbol{\nabla}^s \delta \mathbf{u} : \boldsymbol{\sigma}\, dV \\ &\delta L_{coh} = \int_{\Gamma_c} \delta[[\mathbf{u}]] \cdot \mathbf{t}^{\mathbf{c}} d\Gamma_c, \quad \delta L_{ext} = \int_{\Omega} \delta \mathbf{u} \cdot \mathbf{b} d\Omega + \int_{\Gamma_n} \delta \mathbf{u} \cdot \mathbf{t}\, d\Gamma_n \end{aligned} \tag{5.6}$$

where δ indicates the virtual variation, L_{int}, L_{coh} and L_{ext} refer to the bulk strain energy, work due to the cohesive crack, and external loading, respectively. $[[\mathbf{u}]]$ denotes the displacement jump across the cohesive surface,

$$[[u_i]] = u_i^+ - u_i^- \tag{5.7}$$

where u_i^+ and u_i^- denote the displacement of the given point i on the upper (Ω_+) and lower surface (Ω_-) of the interface.

The cohesive constitutive law describes the relationship between the cohesive traction τ_i and the displacement jump Δ_i across the interface,

$$\tau_j = D_{ji}\, \Delta_i \tag{5.8}$$

where D_{ji} is the constitutive operator and Δ_i is the displacement jump across the interface in the local coordinate system. Formulated within the context of the damage mechanics, the free energy density Ψ reads [27, 31]

$$\Psi(\Delta, d) = (1-d)\Psi^0(\Delta) - d\Psi^0(\delta_{3i}\langle -\Delta_3 \rangle) \tag{5.9}$$

where Ψ^0 is the free energy per unit surface. δ_{ij} is the Kronecker delta and d is the scalar damage parameter accounting for decohesion. The operator $< . >$ used in Eq. 5.9 is $< x >= \frac{1}{2}(x + |x|)$. By differentiating Eq. 5.9),

$$\tau_i = (1-d) D_{ij}^0 \Delta_j - d\, D_{ij}^0 \delta_{3j} \langle -\Delta_3 \rangle \tag{5.10}$$

where D_{ij}^0 is the undamaged stiffness tensor expressed in terms of the input penalty parameter. Under mixed-mode loading, the decohesion onset follows the quadratic criterion proposed by Ye [33],

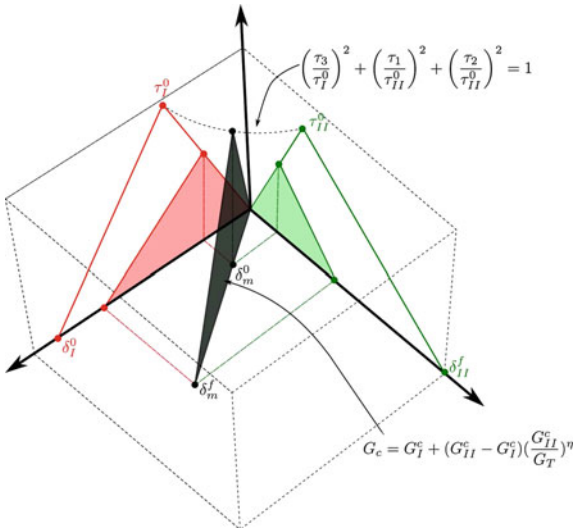

Fig. 5.2 Mixed-mode cohesive criteria

$$\left(\frac{<\tau_3>}{\tau_I^0}\right)^2+\left(\frac{\tau_1}{\tau_{II}^0}\right)^2+\left(\frac{\tau_2}{\tau_{II}^0}\right)^2=1 \tag{5.11}$$

where τ_i refers to the cohesive traction in direction i, τ_I^0 and τ_{II}^0 are the cohesive strengths under mode I and mode II, receptively. A bilinear constitutive law defines the cohesive traction and displacement jump [21]. The damage propagation criteria uses the expression for the critical energy release rate for mixed-mode proposed by Benzeggagh and Kenane [3],

$$G_c = G_I^c + (G_{II}^c - G_I^c)\left(\frac{G_I^c}{G_T}\right)^\eta; \quad G_T = \frac{G_{II}}{G_I + G_{II}} \tag{5.12}$$

where G_I^c and G_{II}^c are the critical energy release rates under mode I and mode II, respectively. η is an experimentally fitted parameter. As illustrated in Fig. 5.2, the area under the traction-displacement jump relation equals to the fraction toughness G_c.

5.3 Structural Theories and Finite Element Formulation

Within the 1D CUF formulation, $\mathbf{u}\,(x, y, z)$ becomes a generic expansion of primary unknowns as follows:

$$\mathbf{u}\,(x, y, z) = F_\tau(x, z)\,\mathbf{u}_\tau(y) \quad \forall \quad \tau = 1, 2, \ldots, M \tag{5.13}$$

where F_τ is the expansion function that defines the kinematic field on $x - z$ with M number of terms. $\mathbf{u}_\tau(y)$ is the vector of generalized displacements along the beam axis. The choice of the expansion function determines the class of 1D CUF models. This chapter deals with two classes of expansion functions, namely (a) Taylor Expansion (TE) and (b) Lagrange Expansion (LE). TE employ Maclaurin polynomials of the kind $x^i z^j$ [6], whereas LE use Lagrange polynomials [7]. Unlike TE, LE have pure displacement variables as detailed in [9]. The discretization along the y-axis follows the Finite Element Method (FEM),

$$\mathbf{u}\,(x, y, z) = N_i(y)\; F_\tau(x, z)\; \mathbf{u}_{\tau i}(y) \qquad \forall \quad \tau = 1, \ldots, M \quad i = 1, \ldots p+1 \tag{5.14}$$

$$\mathbf{u}_{\tau i} = [u_{x_{\tau i}}\; u_{y_{\tau i}}\; u_{z_{\tau i}}] \tag{5.15}$$

where N_i is the ith shape function of order p [2] and $\mathbf{u}_{\tau i}$ is the FE nodal vector. Numerical results employed three types of beam elements, B2 (two nodes), B3 (three nodes) and B4 (four nodes) leading to linear, quadratic and cubic approximations, respectively. The choice of shape functions used along the beam axis remains independent of the expansions employed for the cross-section.

5.3.1 Nonlinear Governing Equations

Within a nonlinear FEM context, the original problem becomes a set of incremental finite element equations solved at definite step instances,

$$\mathbf{f}_{int}(\mathbf{u}) - \mathbf{f}_{ext} = 0 \tag{5.16}$$

where $\mathbf{f}_{int}$ is the global internal force vector which is a function of global finite element displacement vector $\mathbf{u}$ and $\mathbf{f}_{ext}$ refers to the external force vector. In CUF, finite element arrays are

$$\mathbf{k}^S_{ij\tau s}\mathbf{u}_{\tau i} - \mathbf{p}_{sj} = 0 \tag{5.17}$$

where $\mathbf{k}_s^{ij\tau s}$ and $\mathbf{p}_{sj}$ refer to Fundamental Nuclei (FNs) of the secant stiffness matrix and the nodal loading vector, respectively. The strain vector relates to the generalized nodal unknowns via the differential operator of Eq. 5.3,

$$\boldsymbol{\varepsilon} = \mathbf{B}_{\tau i}\; \mathbf{u}_{\tau i} \qquad \mathbf{B}_{\tau i} = \mathbf{b}(N_i F_\tau) = \begin{bmatrix} N_i F_{\tau,x} & 0 & 0 \\ 0 & N_{i,y} F_\tau & 0 \\ 0 & 0 & N_i F_{\tau,z} \\ 0 & N_i F_{\tau,z} & N_{i,y} F_\tau \\ N_i F_{\tau,z} & 0 & N_i F_{\tau,x} \\ N_{i,y} F_\tau & N_i F_{\tau,x} & 0 \end{bmatrix} \tag{5.18}$$

Analogously for virtual variations,

$$\delta\boldsymbol{\varepsilon} = \mathbf{B}_{sj}\,\delta\mathbf{u}_{sj} \tag{5.19}$$

The strain energy becomes

$$\delta L_{int} = \delta\mathbf{u}_{sj}\int_V \left\{\mathbf{B}_{sj}^T C^S \mathbf{B}_{\tau i}\,dV\right\}\mathbf{u}_{\tau i} = \delta\mathbf{u}_{sj}\mathbf{k}_{ij\tau s}^S\mathbf{u}_{\tau i} \tag{5.20}$$

where C^S is the secant material matrix and the secant matrix $\mathbf{k}_{ij\tau s}^S$ is of size 3×3,

$$\mathbf{k}_{ij\tau s}^S = \begin{bmatrix} k_{ij\tau s}^{xx} & k_{ij\tau s}^{xy} & k_{ij\tau s}^{xz} \\ k_{ij\tau s}^{yx} & k_{ij\tau s}^{yy} & k_{ij\tau s}^{yz} \\ k_{ij\tau s}^{zx} & k_{ij\tau s}^{zy} & k_{ij\tau s}^{zz} \end{bmatrix} \tag{5.21}$$

Diagonal and off-diagonal terms have recurrent expressions stemming from the following:

$$\begin{aligned} k_{ij\tau s}^{xx} &= (C_{11}^S F_{s,x}N_j + C_{51}^S F_{s,z}N_j + C_{61}^S F_s N_{j,y})F_{\tau,x}N_i + (C_{15}^S F_{s,x}N_j + C_{55}^S F_{s,z}N_j + \\ &\quad C_{65}^S F_s N_{j,y})F_{\tau,z}N_i + (C_{16}^S F_{s,x}N_j + C_{56}^S F_{s,z}N_j + C_{66}^S F_s N_{j,y})F_\tau N_{i,y} \\ k_{ij\tau s}^{xy} &= (C_{12}^S F_{s,x}N_j + C_{52}^S F_{s,z}N_j + C_{62}^S F_s N_{j,y})F_\tau N_{i,y} + (C_{14}^S F_{s,x}N_j + C_{54}^S F_{s,z}N_j + \\ &\quad C_{64}^S F_s N_{j,y})F_{\tau,z}N_i + (C_{16}^S F_{s,x}N_j + C_{56}^S F_{s,z}N_j + C_{66}^S F_s N_{j,y})F_{\tau,x}N_i \end{aligned} \tag{5.22}$$

The virtual variation of external work is

$$\delta L_{ext} = \int_V \delta\mathbf{u}^T\mathbf{g}dV + \int_S \delta\mathbf{u}^T\mathbf{q}dS + \int_l \delta\mathbf{u}^T\mathbf{r}dl + \delta\mathbf{u}^T P_m \tag{5.23}$$

where $\mathbf{g}$, $\mathbf{q}$, $\mathbf{r}$ and P_m are body forces per unit volume, surface forces per unit area, line forces per unit line and concentrated forces acting at point m, respectively. Within the scheme of 1D CUF, the external load vector becomes

$$\mathbf{p}_{sj} = \int_V N_j F_s\,\mathbf{g}\,dV + \int_S N_j F_s\,\mathbf{q}\,dS + \int_l N_j F_s\,\mathbf{r}\,dl + N_j F_s P_m \tag{5.24}$$

For a generic, arbitrary higher-order beam elements of order p and expansion functions with M terms, the global assembly exploits the expanding indices of FN $\tau, s = 1, 2, \ldots M$ and $i, j = 1, 2, \ldots p+1$,

$$\mathbf{K}^S = \sum_{n=1}^{n_{elem}}\sum_{i,j=1}^{p+1}\bigcup_{\tau,s=1}^{M} k_{ij\tau s}^S \quad \mathbf{f}_{int} = \sum_{n=1}^{n_{elem}}\sum_{i=1}^{p+1}\bigcup_{\tau=1}^{M} f_{int_{\tau i}} \quad \mathbf{p} = \sum_{n=1}^{n_{elem}}\sum_{j=1}^{p+1}\bigcup_{s=1}^{M} p_{\tau i} \tag{5.25}$$

where $\sum$ is the finite element assembly operator that sum the corresponding contributions from all the elements based on the order of FE for given shared DOF.

$\bigcup$ is the CUF assembly operator which sums the corresponding contributions based on the theory of structure. $\mathbf{K}^S$, $\mathbf{f}_{int}$ and $\mathbf{p}$ are the global assembled secant stiffness matrix, global internal force vector and global external load vectors, respectively. The internal force vector derives from the multiplication of the stiffness matrix and the current displacement field. Therefore, Eq. 5.17 becomes

$$\mathbf{K}^S\mathbf{u} = \mathbf{p} \tag{5.26}$$

Readers are referred to the book by Carrera et al. [9] for detailed information on assembly procedure within CUF framework.

5.3.2 CUF Cohesive Elements

Within CUF, the displacement field on the upper and lower faces of the cohesive Lagrange element is

$$\mathbf{u}^+ = F_\tau N_i \mathbf{u}^+_{\tau i} \qquad \mathbf{u}^- = F_\tau N_i \mathbf{u}^-_{\tau i} \qquad [[\mathbf{u}]] = F_\tau N_i \, (\mathbf{u}^+_{\tau i} - \mathbf{u}^-_{\tau i}) \tag{5.27}$$

where $\mathbf{u}^+$ and $\mathbf{u}^-$ are the displacement along the upper and lower edge of the CS element, respectively. Figure 5.3 shows three classes of cohesive Lagrange cross-section element, namely, (a) four-node CS4—linear, (b) six-node CS6—quadratic, and (c) eight-node CS8—cubic. Therefore, the fundamental nuclei of cohesive forces become

$$f^+_{coh_{\tau i}} = \int_{\Gamma_c} F_\tau N_i \, \mathbf{u}^+_{\tau i} \, t^+ d\Gamma_c \quad f^-_{coh_{\tau i}} = \int_{\Gamma_c} F_\tau N_i \, \mathbf{u}^-_{\tau i} \, t^- d\Gamma_c \tag{5.28}$$

The derivation of the fundamental nuclei of the cohesive tangent nucleus makes use of a generic constitutive cohesive law in the rate form,

$$\dot{\mathbf{t}}^c = \mathbf{Q}\,\mathbf{D}\,\mathbf{Q}^T[[\dot{\mathbf{u}}]] = \mathbf{Q}\,\mathbf{D}\,\mathbf{Q}^T \; F_\tau N_i \, (\mathbf{u}^+_{\tau i} - \mathbf{u}^-_{\tau i}) \tag{5.29}$$

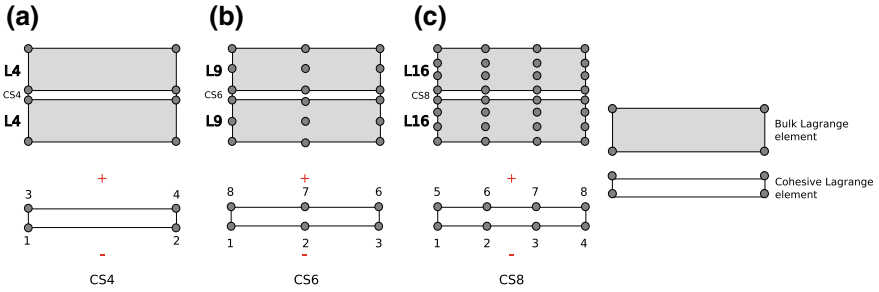

Fig. 5.3 Cohesive Lagrange cross-section elements

where $\mathbf{D}$ is the cohesive tangent material matrix along with orthogonal transformation matrix $\mathbf{Q}$. The fundamental nuclei for the cohesive tangent matrix stems from the linearization of the cohesive force vector (Eq. 5.28),

$$\mathbf{k}_{\mathbf{ij\tau s}}^{\mathbf{coh}} = \int_{\mathbf{c}} \mathbf{F}_{\tau}\mathbf{N}_{\mathbf{i}}\mathbf{Q}\,\mathbf{D}\,\mathbf{Q}^{\mathbf{T}}\mathbf{F}_{\mathbf{s}}\mathbf{N}_{\mathbf{j}}\mathbf{d}_{\mathbf{c}} \tag{5.30}$$

5.4 Nonlinear Solution Schemes

The nonlinear nature of the set of algebraic equations formulated in Eq. 5.16 necessitates iterative schemes such as the Newton-Raphson method (NR),

$$\boldsymbol{\phi}_{res} = \mathbf{K}^{S}\mathbf{u} - \mathbf{p} \tag{5.31}$$

where $\boldsymbol{\phi}_{res}$ is the unbalanced residual nodal vector. Next step requires the truncation of the Taylor series expansion to linear terms of $\boldsymbol{\phi}_{res}$ about a known solution $(\mathbf{u}, \mathbf{p})$,

$$\begin{aligned}\boldsymbol{\phi}_{res}(\mathbf{u}+\delta\mathbf{u}, \mathbf{p}+\delta\mathbf{p}) &= \boldsymbol{\phi}_{res}(\mathbf{u}, \mathbf{p}) + \frac{\partial\boldsymbol{\phi}_{res}}{\partial\mathbf{u}}\delta\mathbf{u} + \frac{\partial\boldsymbol{\phi}_{res}}{\partial\mathbf{p}}\delta\lambda\mathbf{p} = 0 \\ &= \boldsymbol{\phi}_{res}(\mathbf{u}, \mathbf{p}) + \mathbf{K}^{T}(\mathbf{u})\delta\mathbf{u} - \delta\lambda\mathbf{p} = 0\end{aligned} \tag{5.32}$$

where $\mathbf{K}^{T}(\mathbf{u})$ is the tangent stiffness matrix and λ is the load parameter ($\mathbf{p} = \lambda\mathbf{p}_{ref}$). Accounting for additional sets of constraint relationships for the load-scaling parameter λ within the global system of equation, the matrix form of Eq. 5.32 becomes

$$\begin{bmatrix}\mathbf{K}^{tan} & -\mathbf{p} \\ \mathbf{h}^{T} & s\end{bmatrix}\begin{bmatrix}\delta\mathbf{u} \\ \delta\lambda\end{bmatrix} = \begin{bmatrix}\boldsymbol{\phi}_{res} \\ -g\end{bmatrix} \tag{5.33}$$

where g is the path following constraint equation. $\mathbf{h}$ and scalar s are

$$g(\mathbf{u}_0, \lambda_0, \delta\mathbf{u}, \delta\lambda) = 0; \qquad \mathbf{h} = \frac{\partial g}{\partial\mathbf{u}}; \qquad s = \frac{\partial g}{\partial\lambda} \tag{5.34}$$

The constraint equation depends on the incremental scheme adopted. Standard incremental schemes, such as the displacement-control method, require $g(\delta\mathbf{u}, \delta\lambda) = 0$, whereas, load-controlled methods require $\delta\lambda = 0$. Based on the pioneering work of Riks, numerical strategies based on arc-length techniques are of interest to characterize complex equilibrium paths [24] and are powerful for nonlinear elastic problems [5]. Traditional arc-length techniques often fail when the analysis involves material instabilities with localized failure. Gutiérrez introduced a path-following constraint based on the energy-released rate for geometrically linear continuum damage models [15]. Based on the assumption that the unloading behavior remains elastic, the dissipation-based arc-length constraint equation is

$$g = \frac{1}{2}\mathbf{p}^T(\lambda_0 \Delta\mathbf{u} - \Delta\lambda\mathbf{u}_0) - \Delta\tau \tag{5.35}$$

where λ_0 and $\mathbf{u}_0$ are the last converged load factor and displacement vector and $\Delta\tau$ is the path parameter. The derivatives required for the construction of the global consistent tangent matrix (Eq. 5.33) read [32]

$$\mathbf{h} = \frac{\partial g}{\partial \mathbf{u}} = \frac{1}{2}\lambda_0\mathbf{p}^T, \qquad s = \frac{\partial g}{\partial \lambda} = -\frac{1}{2}\mathbf{p}^T\mathbf{u}_0 \tag{5.36}$$

The derivatives yield additional consistent tangent terms independent of the displacement and load increment, thereby making it computationally attractive.

At each NR iteration, the system of equations is

$$\begin{bmatrix} \mathbf{K}^{tan} & -\mathbf{p} \\ \mathbf{h}^T & s \end{bmatrix} \begin{bmatrix} d\mathbf{u} \\ d\lambda \end{bmatrix} = \begin{bmatrix} \boldsymbol{\phi}_{res}^k \\ -g^k \end{bmatrix}; \qquad \begin{bmatrix} d\mathbf{u} \\ d\lambda \end{bmatrix} = \begin{bmatrix} \Delta\mathbf{u} \\ \Delta\lambda \end{bmatrix}^{k+1} - \begin{bmatrix} \Delta\mathbf{u} \\ \Delta\lambda \end{bmatrix}^{k} \tag{5.37}$$

where k refers to the previous iteration and $\Delta\mathbf{u}$ and $\Delta\lambda$ are the displacement and load increments, respectively. It is evident from the Eq. 5.37 that the banded structure of the global consistent tangent matrix deteriorates due to the presence of additional terms pertaining to constraint equations. Using the Sherman-Morrison formula, the global consistent tangent (Eq. 5.37) becomes [26, 32]

$$\begin{bmatrix} d\mathbf{u} \\ d\lambda \end{bmatrix} = \begin{bmatrix} \mathbf{d}^I \\ -g^k \end{bmatrix} - \frac{1}{\mathbf{h}^T\mathbf{d}^{II} - s} \begin{bmatrix} (\mathbf{h}^T\mathbf{d}^I + g^k)\mathbf{d}^{II} \\ -\mathbf{h}^T\mathbf{d}^I - g^k(1 + \mathbf{h}^T\mathbf{d}^{II} - s) \end{bmatrix} \tag{5.38}$$

where the vectors $\mathbf{d}^I$ and $\mathbf{d}^{II}$ stem from the factorization of the structural tangent matrix $\mathbf{K}^{tan}$,

$$\mathbf{K}^{tan}\,\mathbf{d}^I = \boldsymbol{\phi}_{res} \qquad \mathbf{K}^{tan}\,\mathbf{d}^{II} = -\mathbf{p} \tag{5.39}$$

The amount of energy dissipated during a given load increment is always a monotonically increasing quantity. However, the solver can run into numerical issues at non-dissipative regions—such as pure elastic loading—on the equilibrium path as the path parameter can approach the machine precision. The addition of a robust switching algorithm based on the introduction of threshold values can alleviate this problem. The algorithm switches to displacement/force controlled loading in non-dissipative regions and switches back to dissipation-controlled according to the energy threshold. In addition, the path parameter $\Delta\tau$ needs adjustments during the course of computation to limit the number of steps. The adjustment is automatic via setting the optimal value of iterations per increment k_{opt}. The path parameter for a given increment i is [15]

$$\Delta\tau^i = \Delta\tau^{i-1}\frac{k_{opt}}{k^{i-1}} \tag{5.40}$$

where k^{i-1} refers to the number of iterations required in the last converged load step.

5.5 Numerical Applications

This section presents three numerical examples to assess the efficiency of higher-order models. The first example deals with a multilayered cantilever beam under bending with physical nonlinearities modeled through the von Mises plasticity model. The second numerical case deals with the delamination of a double cantilever beam test through the cohesive-based models. A numerical case based on the nonlinear micromechanical framework is the third numerical case.

5.5.1 Multilayered Cantilever Beam Under Bending

This example uses two configurations, (a) asymmetric two-layered and (b) symmetric three-layered, see Fig. 5.4. Classical beam models–EBBT and TBT—and the linear TE model (TE1) provide accurate responses in the linear regime whereas the lack of accurate stress resolution invalidates their effectiveness beyond the elastic limit. The results are consistent with findings by Carrera et al. for monolayered cantilever beam examples [8]. Figure 5.4 and Table 5.1 show comparisons against 3D FEM solutions

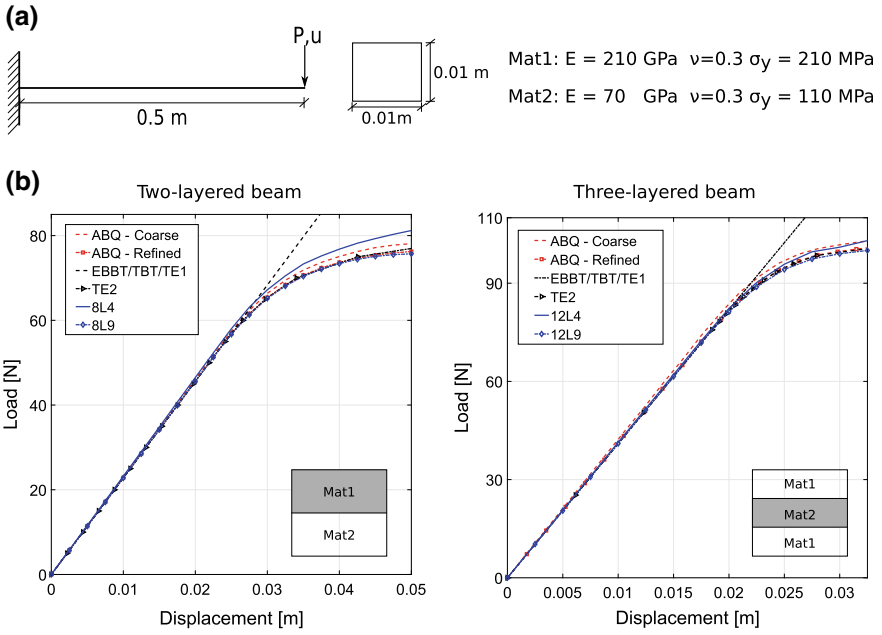

Fig. 5.4 Nonlinear response of multilayered cantilever beam under bending: **a** Geometry, boundary condition and material properties of the multilayered beam and **b** Comparison of equilibrium path for two-layered and three-layered beam configuration using various models

Table 5.1 Comparison of maximum accumulated equivalent plastic strain for different models for the multi-layered cantilever beam under bending

Model	Two layers		Three layers	
	DOF	$\bar{\varepsilon}_p^{max}[\times 10^{-3}]$	DOF	$\bar{\varepsilon}_p^{max}[\times 10^{-3}]$
3D FE models				
ABQ-Coarse	21084	7.66	42210	4.79
ABQ-Refined	64260	8.07	63210	4.89
TE models				
EBBT	363	–	363	–
TBT	605	–	605	–
TE1	1089	–	1089	–
TE2	2178	5.65	2178	3.57
LE models				
8L4[a]/12L4[b]	5445	5.35	7623	3.99
8L9[a]/12L9[b]	16335	8.56	23595	4.87

[a]Two layers
[b]Three layers

based on standard 8-node brick elements using ABAQUS with varying mesh density. Higher-order models can capture the nonlinear response with great computational efficiency without deteriorating the accuracy.

5.5.2 Double Cantilever Test

This problem highlights the necessity to capture high-stress gradients and its effects on the overall response. The geometry and boundary conditions along with material properties are in Fig. 5.5a. The beam model has a 4 L9 cross-section along with 2 CS6 cohesive elements interfaced between the layers. DOF for the CUF models are, 6290 for 180B2, 32490 for 360B2, and 16290 for 60B4. Verification makes use of an analytical solution based on a classical beam theory [21]. From Fig. 5.5c, the use of B4 proves to be effective whereas B2 tends to over-predict the results.

5.5.3 Nonlinear Response of Randomly Distributed RVE

This section deals with the inelastic pre-peak nonlinear response of a randomly distributed Representative Volume Element (RVE). Kaleel et al. investigated the pre-peak nonlinear and progressive failure analysis of fiber-reinforced composites for various classes of RVE and material systems based on a nonlinear micromechanical platform [18, 19]. The numerical examples focus on a twelve-fiber randomly distributed RVE equipped with the von Mises plasticity constitutive law to model the shear-driven nonlinear behavior of the matrix. The fiber is linear elastic. As depicted

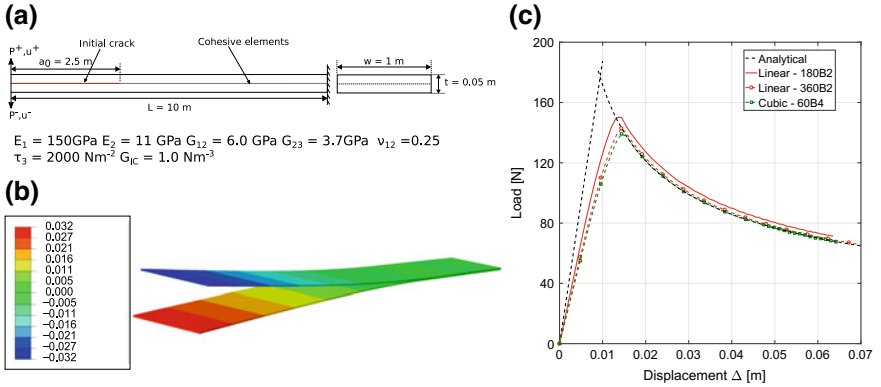

Fig. 5.5 Double cantilever beam test of a composite beam **a** Geometry and material properties of the DCB, **b** 3D deformed configuration for the 60B4 **c** Comparison of equilibrium curves along with analytical solutions

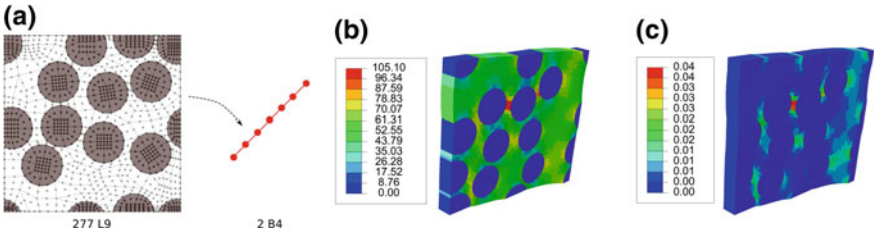

Fig. 5.6 Randomly distributed RVE under applied out-of-plane shear $\bar{\varepsilon}_{13}$ of 0.02 **a** CUF modeling, **b** von Mises stress (σ_{vm}), **c** Accumulated plastic strain

in Fig. 5.6a, the RVE has 277 L9 elements with 2 B4 elements, 24801 DOF, and subjected to an out-of-plane macro shear strain ε_{13} of 0.02 through periodic boundary conditions. The contour plots for the von Mises stress and accumulated plastic strain are in Fig. 5.6b, c, respectively. The results present severe local accumulations of stress and strain requiring higher-order kinematics along the cross-section. Kaleel et al. demonstrated that for the linear elastic homogenization CUF requires a one-order magnitude of DOF less than standard 3D brick elements and multi-fold decrease in computational time in the case of nonlinear analysis [18, 19].

5.6 Conclusion

This chapter has presented results on the nonlinear analysis of structures via refined 1D models. The physical nonlinearities consider plasticity and delamination effects. The structural modeling adopts the CUF to generate 1D models with enriched displacement field. The nonlinear structural analysis may benefit from the use of refined 1D models for two main reasons,

- The proper detection of 3D effects is fundamental to capture local effects due, for instance, to plasticity or delamination onsets. Classical models, such as Euler–Bernoulli and Timoshenko, cannot detect such effects along the cross-section of the structure and may lead to significantly wrong results.
- The need for iterative solution schemes leads to computational overheads limiting the complexity of the structural configuration. The use of 1D models can decrease such an overhead given that 10–100 times less unknown variables than 2D and 3D models are necessary.

As general guidelines, the use of Taylor expansions is recommended when the global response is of interest. The proper detection of highly 3D local effects requires the use of Lagrange expansions. The latter, moreover, have only pure displacements as DOF and can model the geometry and material characteristics of each component of the structure accurately without homogenization procedures.

References

1. Abambres M, Camotim D, Silvestre N (2014) GBT-based elastic-plastic post-buckling analysis of stainless steel thin-walled members. Thin-Walled Struct 83:85–102
2. Bathe KJ (1996) Finite element procedures. Prentice Hall, USA
3. Benzeggagh ML, Kenane M (1996) Measurement of mixed-mode delamination fracture toughness of unidirectional glass/epoxy composites with mixed-mode bending apparatus. Compos Sci Technol 56(4):439–449
4. Bernoulli D (1751) Commentarii academiae scientiarum imperialis petropolitanae, chapter De vibrationibus et sono laminarum. Petropoli
5. Carrera E (1994) A study on arc-length-type methods and their operation failures illustrated by a simple model. Comput Struct 50(2):217–229
6. Carrera E, Giunta G (2010) Refined beam theories based on a unified formulation. Int J Appl Mech 2:117–143
7. Carrera E, Petrolo M (2011) Refined beam elements with only displacement variables and plate/shell capabilities. Meccanica 47:537–556
8. Carrera E, Kaleel I, Petrolo M (2017) Elastoplastic analysis of compact and thin-walled structures using classical and refined beam finite element models. Mech Adv Mater Struct (in press)
9. Carrera E, Cinefra M, Petrolo M, Zappino E (2014) Finite element analysis of structures through unified formulation. Wiley, United Kingdom
10. Cesnik CES, Hodges DH (1997) VABS: a new concept for composite rotor blade cross-sectional modeling. J Am Helicopter Soc 42(1):27–38
11. Eijo A, Oñate E, Oller S (2013) A numerical model of delamination in composite laminated beams using the LRZ beam element based on the refined zigzag theory. Compos Struct 104:270–280
12. Euler L (1744) De curvis elasticis. Bousquet, Geneva
13. Filippi M, Carrera E (2016) Capabilities of 1D CUF-based models to analyse metallic/composite rotors. Adv Aircr Spacecr Sci 3(1):1–14
14. Groh RMJ, Tessler A (2017) Computationally efficient beam elements for accurate stresses in sandwich laminates and laminated composites with delaminations. Comput Methods Appl Mech Eng 320:369–395
15. Gutiérrez MA (2004) Energy release control for numerical simulations of failure in quasi-brittle solids. Commun Numer Methods Eng 20(1):19–29

16. Jiang F, Yu W (2016) Nonlinear variational asymptotic sectional analysis of hyperelastic beams. AIAA J 54(2):679–690
17. Jiang F, Yu W (2017) Damage analysis by physically nonlinear composite beam theory. Compos Struct 182:652–665
18. Kaleel I, Petrolo M, Waas AM, Carrera E (2017) Computationally efficient, high-fidelity micromechanics framework using refined 1D models. Compos Struct 181:358–367
19. Kaleel I, Petrolo M, Waas AM, Carrera E (2018) Micromechanical progressive failure analysis of fiber-reinforced composite using refined beam models. J Appl Mech 85(2)
20. Kaleel I, Petrolo M, Carrera E (2018) Elastoplastic and progressive failure analysis of fiber-reinforced composites via an efficient nonlinear microscale model. Aerotec Missili Spaz 97(2):103–110
21. Mi Y, Crisfield MA, Davies GAO, Hellweg HB (1998) Progressive delamination using interface elements. J Compos Mater 32(4):1246–1272
22. Pagani A, Carrera E (2017) Large-deflection and post-buckling analyses of laminated composite beams by Carrera Unified Formulation. Compos Struct 170:40–52
23. Pollayi H, Yu W (2014) Modeling matrix cracking in composite rotor blades within VABS framework. Compos Struct 110:62–76
24. Riks E (1979) An incremental approach to the solution of snapping and buckling problems. Int J Solids Struct 15(7):529–551
25. Schardt R (1994) Generalized beam theory-an adequate method for coupled stability problems. Thin-Walled Struct 19(2–4):161–180
26. Sherman J, Morrison WJ (1950) Adjustment of an inverse matrix corresponding to a change in one element of a given matrix. Ann Math Stat 21(1):124–127
27. Simo JC, Ju JW (1987) Strain- and stress-based continuum damage models—-i. formulation. Int J Solids Struct **23**(7):821–840
28. Škec L, Jelenić G, Lustig N (2015) Mixed-mode delamination in 2D layered beam finite elements. Int J Numer Methods Eng 104:767–788
29. Timoshenko SP (1921) On the correction for shear of the differential equation for transverse vibration of prismatic bars. Philos Mag Ser 41(6):744–746
30. Timoshenko SP, Gere JM (1991) Mechanics of materials. Springer-Science+Business Media, New York
31. Turon A, Camanho PP, Costa J, Davila CG (2006) A damage model for the simulation of delamination in advanced composites under variable-mode loading. NASA/Tech. Mem. 213277
32. Verhoosel CV, Remmers JJ, Gutiérrez MA (2009) A dissipation-based arc-length method for robust simulation of brittle and ductile failure. Int J Numer Methods Eng 77:1290–1321
33. Ye L (1996) Measurement of mixed-mode delamination fracture toughness of unidirectional glass/epoxy composites with mixed-mode bending apparatus. Compos Sci Technol 56(4):439–449